Generation and Characterization of High Heat-Flux Plasma-Flow for Divertor Simulation Studies Using a Large Tandem Mirror Device

*Y. Nakashima[1)], I. Katanuma[1)], K. Hosoi[1)], H. Ozawa[1)], R. Yonenaga[1)], Y. Higashizono[2)], N. Nishino[3)], M. Yoshikawa[1)], M. Ichimura[1)], T. Imai[1)], T. Kariya[1)], Y. Kiwamoto[1)], R. Minami[1)], Y. Miyata[1)], Y. Yamaguchi[1)], N. Asakura[4)], A. Hatayama[5)], Y. Hirooka[6)], S. Kado[7)], S. Masuzaki[6)], H. Matsuura[8)], N. Ohno[9)], M. Shoji[6)], Y. Ueda[10)]

[1)]Plasma Research Center, University of Tsukuba, Tsukuba, Ibaraki 305-8577, Japan
[2)]RIAM, Kyushu University, 87 Kasuga, Fukuoka 816-8580, Japan
[3)]Graduate school of Engineering, Hiroshima University, Hiroshima 739-8527, Japan
[4)]Japan Atomic Energy Agency, Naka, Ibaraki 311-0193, Japan
[5)]Faculty of Science and Technology, Keio University, Kanagawa 220-8522, Japan
[6)]National Institute for Fusion Science, Oroshi 322-6, Toki 509-5292, Japan
[7)]Department of Nuclear Engineering and Management, The University of Tokyo, Bunkyo, Tokyo 113-8656, Japan
[8)]Graduate school of Engineering, Osaka Prefecture University, Sakai, Osaka 599-8531, Japan
[9)]Graduate school of Engineering, Nagoya University, Furo-cho, Nagoya 464-8603, Japan
[10)]Graduate school of Engineering, Osaka University, 2-1 Yamadaoka, Suita, Osaka 565-0871, Japan

E-mail contact of main author: nakashma@prc.tsukuba.ac.jp

Abstract. This paper describes the detailed results of heat and particle flux generation carried out at an exit of end-mirror of the large tandem mirror device for divertor simulation studies. Along the future research plan of the plasma research center in the University of Tsukuba, new research project on the study of divertor simulation under the environment that closely resemble actual fusion plasmas is started by making use of the advantage of open magnetic field configuration. In a typical hot-ion-mode plasmas ($n_{e0} \sim 2\times10^{18}$ m^{-3}, $T_{i0} \sim 5$ keV), measurements of heat and particle fluxes from the end-mirror have been carried out by using newly installed diagnostic unit which consists of calorimeter and directional probe at the end-mirror exit. In the case of only ICRF heating, the heat-flux density of 0.8 MW/m^2 and the particle-flux density of 10^{22} particles/s•m^2 were achieved over the range of 6 ~ 9 cm in diameter and heat-flux density increases with the RF power. Superimposing ECH pulse of 300 kW into RF plasmas attained the peak heat flux up to 2 MW/m^2 on axis. In the application of the ECH power, the increase of the heat flux was clearly observed and the temporal heat-flux density during ECH injection is achieved to be 9 MW/m^2. This value comes up to the heat load of the divertor plate of ITER, which gives a clear prospect of generating the required heat-flux density for divertor studies by building up heating systems to the end-mirror cell. The present status of designing the device to be introduced as new divertor system and the near term research plan are also described.

1. Introduction

Designing the divertor system is one of the urgent and important subjects for fuel particle control and exhaust of He ash and impurity particles in fusion devices [1]. In ITER discharges, heat load to the divertor plasma-facing components (PFCs) is estimated to be 5-20 MW/m^2 in steady state and more at the transient phase [2]. In order to reduce such high heat-load, a steady tokamak discharge with detached-plasma condition is an important key as an operation scenario of fusion reactors [3]. To solve this issue, various so-called divertor simulators have been developed and a number of experimental approach have been made toward the realization of divertor [4-9]. In most of these devices, however, plasmas are produced by the DC-discharge (arc discharge) using electrodes and do not completely simulate the plasma flow from high temperature tokamak plasmas. This also has a possibility of a significant hurdle to

create the experimental environment for evaluating the influence of the impurity back-stream from the divertor and the sustainment of detached plasma operation in steady state.

In the Plasma Research Center (PRC) of University of Tsukuba, the following two projects are initiated to upgrade our conventional research plan based on the control of plasma potential and radial electric field using wave heating techniques, such as ECH.

(1) Research on improvement of plasma confinement by potential / electric field will be expanded from the core region to the boundary region.
(2) We will introduce new divertor systems (A-Divertor and E-Divertor) to existing tandem mirror device (GAMMA 10) and develop the study of divertor simulation.

In GAMMA 10, a number of plasma production and heating systems with the same scale of present-day fusion devices, such as radio-frequency (RF) wave, microwave and neutral beam injection systems have been equipped and high-temperature plasmas have been produced [10,11]. In the present research, the investigation of the plasma flow from the end-mirror exit of GAMMA 10 is performed to validate its applicability to the divertor simulation studies.

2. Experimental Setup

2.1. GAMMA 10 Device and the Objectives of the Divertor Simulation Project

Figure 1 shows the schematic view of GAMMA 10 tandem mirror device. GAMMA 10 is an effectively axi-symmetrized tandem mirror with minimum-B anchor and mainly separated into four sections, from the central to the end [10]. A central-cell of GAMMA 10 is consist of a cylindrical vacuum chamber of 1 m in diameter and 6 m in length and ten sets of pancake type coils are installed. The magnetic strength in the central-cell midplane is about 0.5 Tesla and two choke coils installed at both ends of the central-cell form a simple mirror configuration with a mirror ratio of nearly 4. In each minimum-B anchor-cell which is connected to the both ends of the central-cell, MHD stabilization of the plasma is preserved by two baseball coils. Initial plasma (hydrogen) is injected from both end of GAMMA 10 and the plasma is built up by using gas puffers and two types of ICRF waves applied at the central-cell. One ICRF wave (RF1) is excited with two NAGOYA-type III antennas and contributes the plasma production and MHD stabilization by propagating the wave to both anchor-cells. Another wave (RF2) excited with two double-half-turn antennas generates a strong ion cyclotron resonance heating (ICRH) and provides the ion heating in the central-cell. In typical ICRF start-up plasmas, plasma ions perpendicularly heated up to ~10 keV by the above ICRF waves and the electron temperature of several tens eV is achieved in the central-cell. Plasma confining potential is produced by ECH using high power gyrotrons at plug/barrier region in the end-mirror cell. The end-loss plasma leaking to the end-cell is plugged with this confining potential. Plasma particles flowing out of the plug/barrier-cell hit the end plates and neutralized gas is pumped out with large-scale cryo-pump system installed on the end-cell [12].

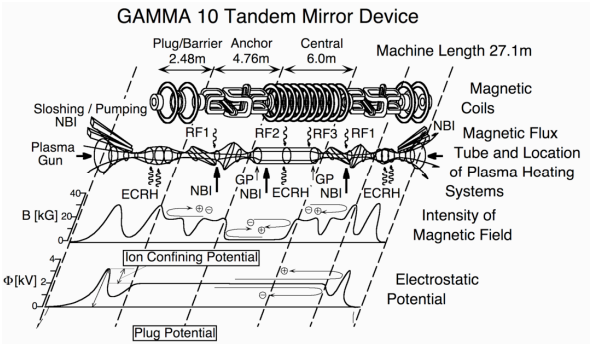

FIG.1. Schematic view of the GAMMA 10 tandem mirror device.

Figure 2 shows the conceptual view of the divertor research project. In this research plan, we develop the new divertor containing a separatrix configuration based on a novel idea (A-Divertor) and a high heat-flux divertor simulator by use of open-ended device (E-Divertor). By using the above devices, we approach the following research subjects of urgency for the ITER project [13].

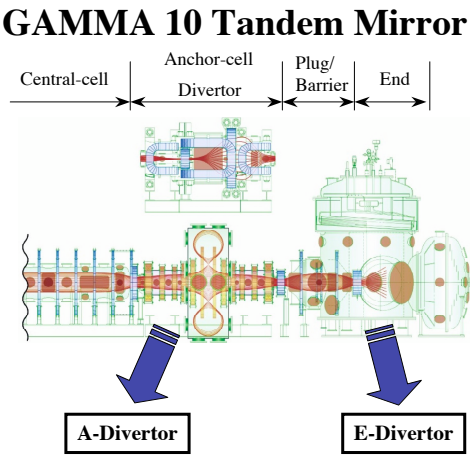

FIG. 2. Conceptual view of the divertor research project.

(a) Plasma-PFC interaction and impurity transport in the divertor region (especially focused on surface physics under ELM-like high heat-flux environment).

(b) Steady-state sustainment of detached plasmas and its physical mechanism (atomic-molecular processes in the divertor plasma, etc.).

(c) Heat and particle control in pedestal and divertor regions.

(d) Divertor pumping and particle exhaust experiments using the large-capacity cryopumping system.

2.2. Diagnostic System

Figure 3 shows the schematic view of the vacuum vessel and the shape of the plasma in the west end-mirror region, together with the location of the diagnostic equipment installed for the E-Divertor experiment. In order to perform a simultaneous measurement of heat and particle fluxes from the end-mirror exit, a set of calorimeter and directional probe was manufactured. Figure 4 (a) shows the assembly photograph of the calorimeter and directional probe. This diagnostic instrument is located at 30 cm downstream from the end-mirror coil (z_{EXIT} = 30 cm) and can be inserted from the bottom of the vacuum vessel up to the center axis of GAMMA 10. This instrument is also capable of rotation around the shaft, which enables to measure the direction of the plasma flow to the magnetic field line.

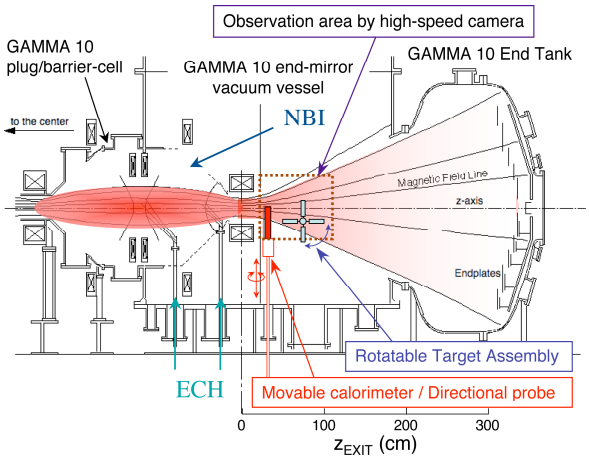

FIG. 3. Schematic view of west end-mirror vacuum vessel and the location of diagnostic instruments for the E-Divertor experiment.

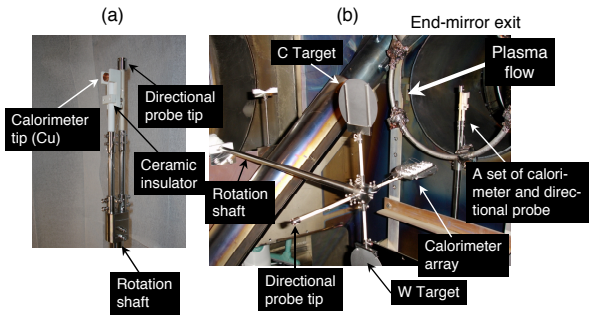

FIG.4. Photograph of the diagnostics. (a) Calorimeter and directional probe. (b) Rotatable target plates.

A set of movable target plates was also made to obtain a visible spectroscopic data from the interactions between the plasma and the target materials. Figure 4 (b) shows the photograph of the assembly of target plates. As shown in the figure, the target plates consist of a 10 cm^{ϕ} carbon disk, a 10 cm^{ϕ} tungsten disk, calorimeter array mounted on the stainless-steel disk and a directional probe. The set of target plates is installed at z_{EXIT} = 70 cm through the horizontal observation port. The target system has a capability of changing the target material by rotating the shaft without the break of air to the vacuum vessel and has a function measuring heat flux and particle flux.

Behaviour of the visible emission from the interaction between plasma and the target materials is observed with high-speed cameras. A high-sensitive CCD camera (HAS-220, DITECT Inc.) or a high-speed camera using CMOS (MEMORECAM GX-1p, NAC Inc.) is mounted on the horizontal port viewing the target. The former camera captured the visible image with 164×228 pixels at 400 frames per second and the latter one took them with 240×320 pixels at 2,000 frames per second. 2-D visible images from both cameras were transferred to data analysis PCs through the network.

3. Experimental Results and Discussion

3.1. Heat and Particle Flux Measurements

3.1.1. Characteristics of ICRF Produced Plasmas

In typical hot-ion-mode plasmas ($n_{e0} \sim 2\times10^{18}$ m^{-3}, $T_{i0} \sim 5$ keV in the central-cell), measurements of heat and particle fluxes from the end-mirror exit have been carried out. In the experiment, ICRF wave heating of 150 kW, 190 ms for plasma production/heating are applied to the initial plasma injected from a plasma gun at east end. Figure 5 shows the angular dependence of ion-flux density measured with the directional probe at z_{EXIT} = 30 cm together with that of heat flux measured with the calorimeter by rotating the diagnostic instrument in the case of only RF plasmas. Each result shows the quite similar dependence, which indicate that the heat source is dominated by ions flowing out of the end-mirror exit.

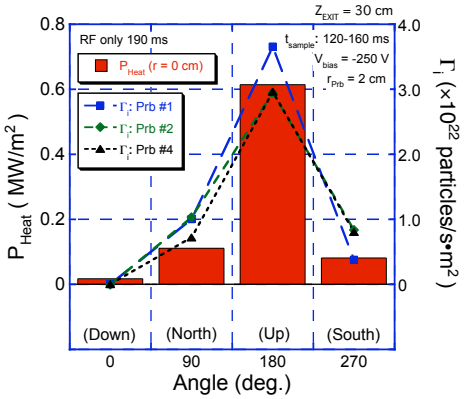

FIG.5. Angular dependence of ion flux and that of heat flux by rotating the diagnostic instrument.

In Fig. 6, the dependence of ICRF power for the ion heating in the central-cell (RF2) on the heat and particle-flux density is presented. As seen in the figure, the heat flux density of 0.8 MW/m^2 and the particle flux density of 4×10^{22} $/s\bullet m^2$ were observed at z_{EXIT} = 30 cm. It is also found that the heat flux density increases almost in proportion to the RF power. However, the particle-flux density near the

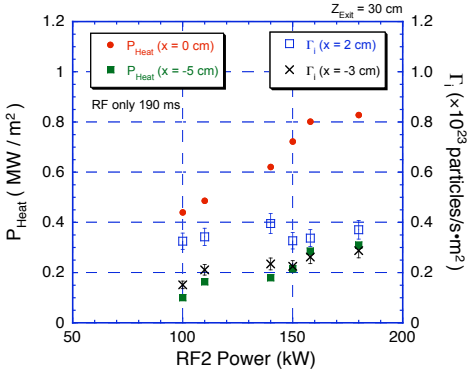

FIG.6. ICRF power dependence of ion flux and that of heat flux.

axis (x = 2 cm) hardly changes with increasing power. This indicates that increase of perpendicular ion energy ($E_{i\perp}$) according to the increase of RF power induces the enhancement of the energy in end-loss ions. In the periphery region, on the other hand, both heat and particle fluxes increase with the RF power. This implies that the radial distribution of the plasma flowing out of the end-mirror exit spreads out with the increase of the RF power.

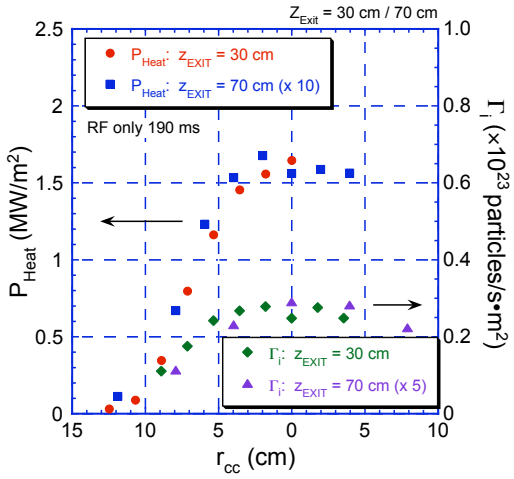

FIG.7. Radial profiles of ion flux and the heat flux. Each position is normalized at the central-cell midplane position.

Figure 7 shows the radial profiles of heat and particle fluxes measured at different positions (z_{EXIT} = 30 and 70 cm). Each position is normalized at the central-cell midplane position according to the shape of the magnetic flux tube. In both profiles, a good agreement is obtained. From the above results, it is confirmed that the spatial distribution of the heat and particle fluxes from the end-mirror exit is governed by the magnetic field configuration in the end-mirror region.

3.1.2. Effect of Superimposing the ECH Pulse

It is well understood that the ECH for potential formation (p-ECH) produces electron flow with high energy along the magnetic field line. Here, the heat flux in additional heating by ECH into the RF produced plasma is evaluated in order to investigate the effect of superimposing the ECH pulse. The radial profile of the heat-flux density measured with the calorimeter is shown in Fig. 8. Here, the ECH pulse with gyrotrons of 150 ~ 300 kW, 20 ~ 25ms are applied to the ICRF produced plasma of 190 ms. As shown in the figure, superimposing the ECH pulse of 300 kW, 25 ms attained the maximum heat-flux up to 2 MW/m^2 on axis. According to the increasing ECH power, the heat flux continues to increase and radial spread of the heat-flux density is also enhanced.

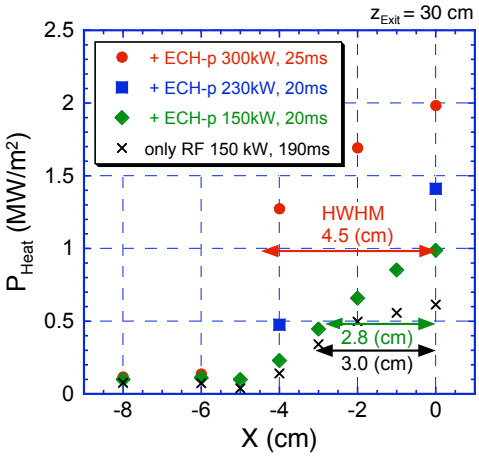

FIG.8. Radial profile of heat flux in the case with superimposing the ECH pulse into RF plasma.

3.2. Visible Image Measurements Using High-Speed Cameras

Initial experiments of plasma irradiation to the target materials installed at 70 cm from the end-mirror exit have been carried out. Figure 9 shows the two-dimensional images of visible emission due to plasma-material interactions obtained from the high-speed camera in cases of a stainless-steel plate mounted with calorimeters made of copper, a tungsten plate and a carbon

plate. In spite of irradiating same flux onto the targets, observed light intensity has large difference in each material.

The time evolution of the visible intensity in the vertical direction observed just front of the target surface is shown in the Fig. 10. It is clearly observed that a rapid reduction of light emission during ECH. This indicates that the ECH injection produces axial plasma confining potential and plugs the end-loss ions. On the other hand, it is also observed at the same time that the supporting shaft of the target made of ceramic is heated during ECH. This implies that the heating effect due to the high-energy electrons produced by the ECH pulse.

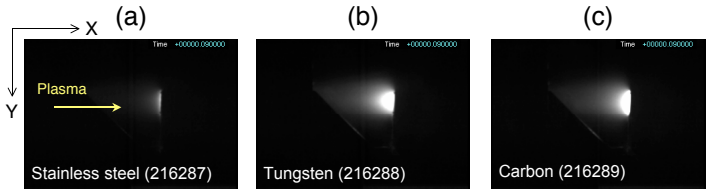

FIG.9. Comparison of 2-D visible image of emission from different target materials. (a) Stainless steel, (b) Tungsten, (c) Carbon.

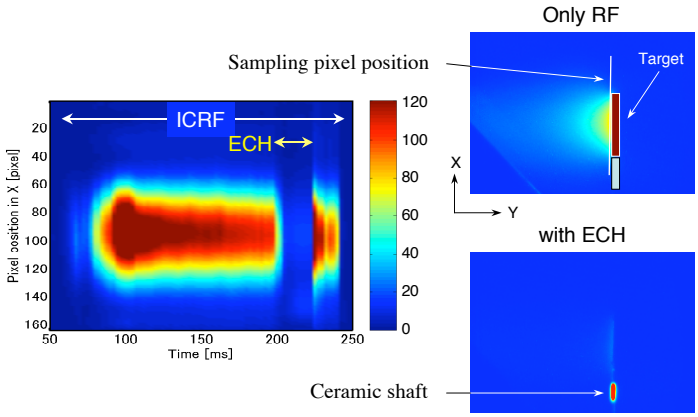

FIG.10. Time evolution of visible emission from the target plates (Stainless-steel).

3.3. Evaluation of the Heat Flux Density During the ECH Pulse

As shown in the previous section, in the period of ECH, effect of end-loss ions is reduced and high-energy electrons play an important role in the plasma material interaction. In the above condition, the net heat-flux density $P_{\mathrm{Heat}}^{\mathrm{net\ ECH}}$ can be evaluated as follows:

$$P_{\mathrm{Heat}}^{\mathrm{net\ ECH}} \equiv \{Q_{\mathrm{Heat}}^{\mathrm{with\ ECH}} - Q_{\mathrm{Heat}}^{\mathrm{only\ RF}} (1 - t_{\mathrm{ECH}} / t_{\mathrm{RF}})\} / t_{\mathrm{ECH}}$$

Here, $Q_{\mathrm{Heat}}^{\mathrm{with\ ECH}}$ is the total calorific value in the plasma discharge with ECH and t_{ECH} is the duration of the ECH pulse. $Q_{\mathrm{Heat}}^{\mathrm{only\ RF}}$ is total calorific value in the only RF plasma and t_{ECH} is its duration.

Figure 11 shows the ECH power dependence on the net heat-flux density in the period of ECH. During 300 kW ECH injection, $P_{\mathrm{Heat}}^{\mathrm{net\ ECH}}$ is estimated to be 9 MW/m^2. This value almost comes up to the heat load of the divertor plate of ITER, which gives a clear prospect of generating the required heat density for divertor studies by building up heating systems to the end-mirror cell.

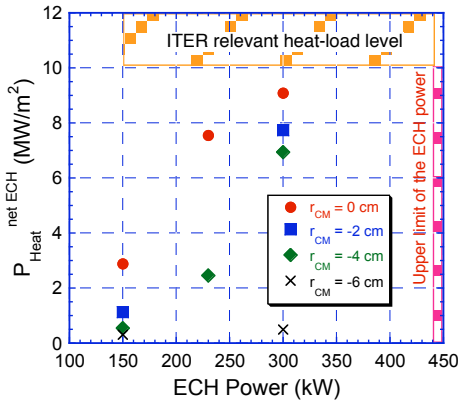

FIG.11. ECH power dependence on the net heat-flux density during ECH.

3.4. Characteristics of Heat and Particle Flux Along the Magnetic Field Line

In similar hot-ion-mode plasmas, heat and particle flux measurement was carried out using a calorimeter and a directional probe mounted on the rotatable target (z_{Exit} = 70 cm) and the results were compared with the results measured near the end-mirror exit (z_{Exit} = 30 cm). Figure 12 shows the axial distribution of the heat-flux density and the particle-flux density measured at the different positions on z-axis in only ICRF plasmas. In the estimation of the heat flux, the measured value is compensated according to the following reflection effect [14].

$$P_{Heat}^{Corrected} \equiv P_{Heat}^{Measured} / (1 - R_E / R_N).$$

Here, R_E and R_N are reflection coefficients of energy and particle, respectively. Based on the corrected heat-flux density and particle-flux density determined from the directional probe measurement, the ion density at the mirror exit is evaluated to be ~3×10^{17} m^{-3}. Data points with connected lines in the figure represent the calculation results of the heat and the particle fluxes by assuming the above ion density and taking into account of the effect of the density reduction due to the expansion of magnetic flux tube in the downstream side from the end-mirror exit. Each value measured at the different axial positions locates between the two calculation lines ($T_{i//}$ = 300 eV and 400 eV). Recent results of energy analysis of end-loss ions measured at the end-cell (Z_{EXIT} = 270 cm) shows that $T_{i//}$ is estimated to be 200 - 400 eV, which gives a good agreement with the calculation. These results indicate that the accuracy of heat and particle flux measurements and that the ion behaviour is fundamentally restricted in the magnetic field configuration.

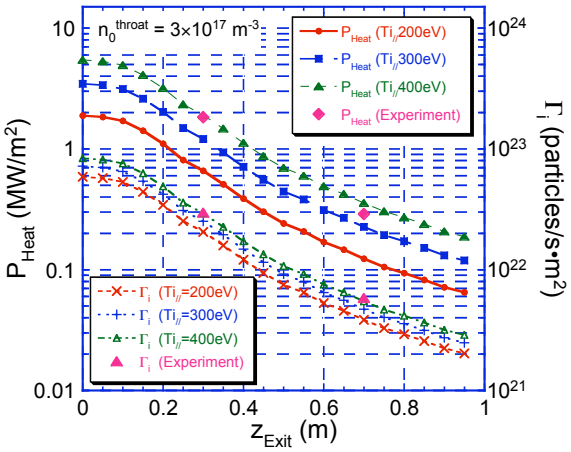

FIG.12. ECH power dependence on the net heat-flux density during ECH.

4. Design of New Divertor System and Near Term Research Plan

In the Plasma Research Center, the following research plan has been considered in near future. As to A-Divertor project, detailed design of the coil system for the axisymmetric divertor configuration has been continued under the optimized condition of MHD stability [15] and compatibility with existing electric power systems. Design of plasma heating systems has been carried out based on the Fokker-Planck simulation [16].

As a research plan for E-Divertor, based on the above shown results, the following experimental issues are planned:

(1) Installation of the divertor experimental-module (D-module) in the end vacuum chamber and generation of strong plasma-surface interactions and realization of plasma detachment using gas injection,

(2) Installation of test material pieces into D-module and high the heat flux plasma irradiation and surface analyses,

(3) Divertor pumping experiment using the large capacity helium cryopumping system.

5. Summary

Divertor simulation study has been started as the new research plan, by the use of a large tandem mirror device. The experiment of the generation of high heat and particle flux is successfully performed at an end-mirror exit of GAMMA 10. In standard hot-ion mode plasmas, the heat-flux density of 0.8 MW/m^2 and the particle-flux density of 4×10^{22}/s•m^2 were observed at 30 cm downstream of the end-mirror exit. It is confirmed that the heat-flux density increases in proportion to the applied RF power. Superimposing the ECH pulse, a remarkable enhancement of heat flux and a peak value in the net heat-flux density of 9 MW/m^2 were attained, which almost comes up to the heat-load level of the ITER divertor plates. Axial and radial profile measurements of heat and particle fluxes showed that the observed heat flux is dominated by ions flowing out of the end-mirror exit and that the end-loss flux is governed by the magnetic field configuration in the end-mirror region. An initial stage of plasma irradiation experiment has been started and a significant change between ECH and RF plasmas is confirmed for the first time in the behaviour of visible emission from the target plates. The above results give a clear prospect of generating the required performance and providing useful information for divertor studies by building up the plasma heating and diagnostic systems to the end-mirror cell.

Acknowledgement

The authors would like to acknowledge the members of the GAMMA 10 group, University of Tsukuba for their collaboration in the experiments. This work was performed with the support by the bi-directional collaboration research programs (NIFS09KUGM037 and NIFS04KUGM009).

References

[1] Roth, J., et al., J. Nucl. Mater. **390-391** (2009) 1.
[2] Fundamenski, W., et al., ibid. 10.
[3] Matthews, G. F., J. Nucl. Mater. **220-222** (1995) 104.
[4] Goebel, D. M., et al., Nucl. Fusion 28 (1988) 1041.
[5] Hirooka, Y., et al., J. Vac. Sci. Technol. A8 (1990) 1790.
[6] Masuzaki, S., et al., Jpn. J. Appl. Phys. **29** (1990) 2835.
[7] Ohno, N., et al., Nucl. Fusion **41** (2001) 1055.
[8] Koch, B., et al., J. Nucl. Mater **290-293** (2001) 653.
[9] Groot, B. de, et al., Fusion Engineering and Design, **66-68** (2003) 413.
[10] Inutake, M., et al., Phys. Rev. Lett. **55** (1985) 939.
[11] Tamano, T., Phys. Plasmas **2** (1995) 2321.
[12] Nakashima, Y., et al., Vacuum **41** No.4-6 (1990) 1561.
[13] Nakashima, Y., et al., to be published in Fusion Eng. Design (2011).
[14] Behrisch, R. and Eckstein, W., *Physics of Plasma-Wall Interactions in Controlled Fusion*, pp. 413-438, Post, D. and Behrisch, R.. Ed., Plenum Press, New York (1986).
[15] Katanuma, I., et al., J. Phys. Soc. Jpn. **69**, No.10 (2000) 3244.
[16] Katanuma, I., Phys. Fluids, **30**, No.4 (1987) 1142.